Chapter - 3

Effect of L-Cysteine on Structural, Thermal, Electrical and Optical Properties of Potassium Dihydrogen Phosphate (KDP)

Chapter-3: Effect of L-Cysteine on Structural, Thermal, Electrical and Optical Properties of Potassium Dihydrogen Phosphate (KDP)

1. Introduction:

Crystal growth plays a vital and significant role in the area of experimental materials science and engineering. It is also necessary for fundamental data acquisition and practical devices such as detectors, integrated circuits, and other applications. Ferroactive crystals have now been identified as nearly indispensable in the field of non-linear optical applications. In particular, KDP (KH_2PO_4), the subject crystal of this study, stands out in this regard. Single crystal growth and characterization are needed to understand its properties, to enhance or modify them [1-2]. Doping of amino acids in KDP (and similar) crystals is known to have a moderate to a significant impact on their properties [3]. In this chapter, the effect of L-Cysteine doping on KDP is discussed.

L-Cysteine is unusual among amino acids as it has a sulfhydryl group in its molecular structure, making it highly reactive. It also serves as a strong reducing factor, while its chirality would expectedly enhance the charge asymmetry feature of the non-centro symmetric crystal. At room temperature, single crystals of KDP are paraelectric, with a strong non-linear optical coefficient, good structural quality, and mechanical properties. The paraelectric phase of KDP has a tetragonal unit cell with parameters, a=b=7.448Å and c=6.977Å. It offers high transmittance across the visible spectral region while still meeting the criteria for optical birefringence large enough to bracket the refractive index for even the most extreme wavelengths [4]. The crystal can endure repeated exposure to a high-power density laser without inducing strains and subsequent inhomogeneities in the refractive index [5]. These properties make it suitable as an efficient tuned dielectric medium for optical harmonic generation in and near the visible field. It can be used for frequency doubling and mixing a wide range of laser wavelengths between 1060nm and 525nm [6-9]. It is important to note that its acousto-optic application is superior to other current deep UV materials. In the deep UV region, it has high transparency. It also significantly manifests the quadratic electro-optic effect. Its only disadvantage is its instability due to its hygroscopic nature, requiring more stringent device packaging [10-11].

Since amino acids have NLO properties, they have been a prominent dopant for potassium dihydrogen phosphate (KDP). They have several unique properties, such as **(i)**

molecular chirality, which ensures non-centrosymmetric crystal structure, **(ii)** absence of strongly conjugated bonds, the feature that leads to wide transparency range in the visible and ultraviolet (UV) spectral regions and **(iii)** Zwitterionic nature of the molecule that favours crystal hardness for applications in devices [12]. Inorganic salts with complexes of amino acids are considered novel materials for Second Harmonic Generation (SHG). They are found to be as promising as KDP or even better in most cases [13,14]. In this study, we have used 1 mol% and 2 mol% L-Cysteine for the doping. Crystals grown from aqueous solution were characterized using Powder X-ray diffraction (XRD), Thermogravimetric Analysis (TGA), Dielectric measurements, Photoluminescence (PL) Analysis, Fourier Transform Infrared (FTIR) Spectroscopy and Ultraviolet-Visible (UV-Visible) Spectroscopy, and they were grown with an aim to investigate modifications in the crystals' physicochemical properties.

2. Experimental:

KDP and L-Cysteine used for growing crystals were both AR grade. Seed crystals obtained over 2-4 days at room temperature were grown using a slow evaporation technique with a saturated aqueous solution of KDP and L-Cysteine (1 mol% and 2 mol%). The growth rate of doped crystals was found to be higher than that of the pure crystals. Fairly grown crystals were harvested after 28-30 days. Figure 1 displays the pure and doped KPD crystals that were obtained. The other crystals had a similar overall appearance. The transparency of both doped and pure crystals was found to be fair to good. In comparison to pure KDP crystals, the doped crystals had an elongated appearance along the c-axis.

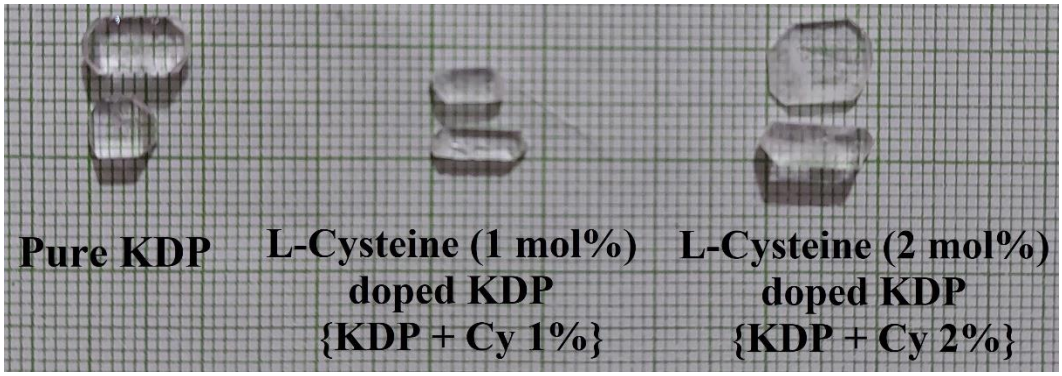

Figure 1. As grown crystals of pure and L-Cysteine doped KDP

3. Results and Discussion:

3.1 Powder XRD Analysis:

Figure 2(a) shows the XRD patterns of pure and L-Cysteine doped KDP crystals. To confirm the crystalline phase of the crystal, powdered samples were scanned in increments of 0.10 seconds within 2θ range of 10°-80°. The powder XRD patterns of KDP and L-Cysteine doped KDP crystals indicate that they belong to the tetragonal system with space group $1\bar{4}2d$. In order to index and evaluate XRD patterns, FullProf suite software was used, and the calculated cell parameters are listed in table 1.

The results confirmed the tetragonal structure of pure and doped KDP crystals, and the slight changes in cell parameters indicate that L-Cysteine affects the crystal lattice of KDP [12]. This suggests that crystals maintain almost a single-phase structure and show only minor variations in unit cell parameters when added L-Cysteine. The intensities of different diffraction patterns are observed to change due to doping. The slight changes in peak position and intensities indicate the successful incorporation of L-Cysteine into the KDP lattice. Sharp diffraction peaks suggest that the doped KDP crystal is free of structural grain boundaries and excellent crystalline nature. Varying the valency of dopants can also result in a variety of strain-related defects. There is a definite trend of peak shifting to increased 2θ with dopant increasing as shown in figure 2(b); however, this shift can be affirmative, though too small.

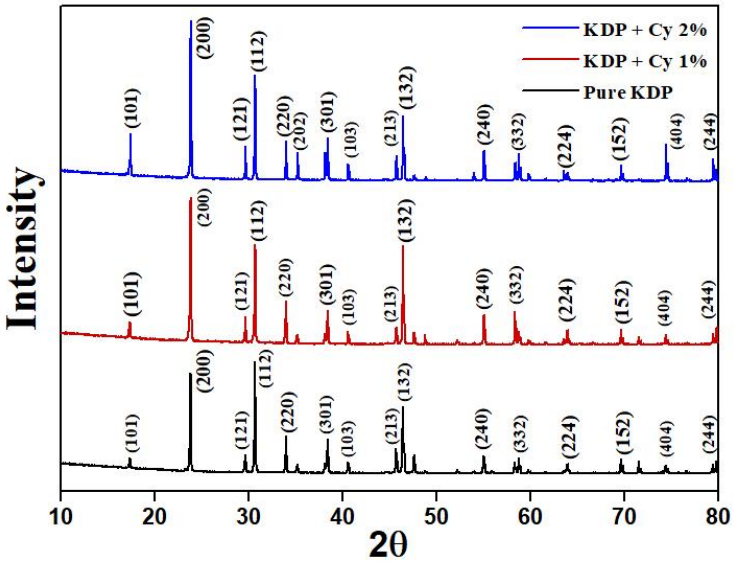

Figure 2(a). XRD pattern of pure and L-Cysteine doped KDP crystals

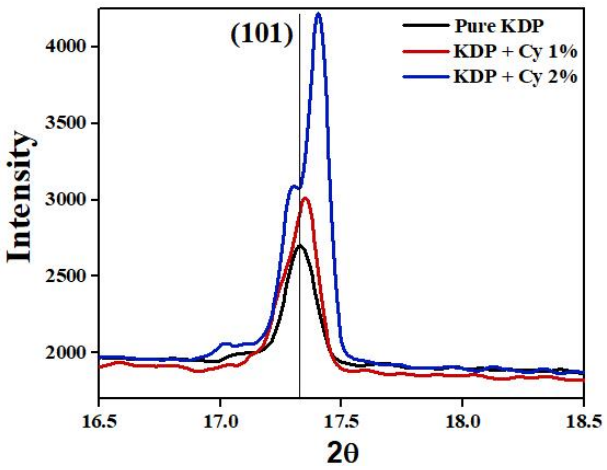

Figure 2(b). Peak (101) shifting of pure, and L-Cysteine doped KDP crystals

Table 1. Lattice parameters of pure & L-Cysteine doped KDP crystals

Crystals	a (Å)	b (Å)	c (Å)	Symmetry
Reported KDP	7.448	7.448	6.977	Tetragonal
KDP+Cy1	7.452	7.452	6.975	
KDP+Cy2	7.458	7.458	6.975	

Table 2. Structural parameters of pure and doped KDP crystals

Sample	FWHM	2θ	Crystallite Size t (nm)	Strain ε ($lin^{-2}\ m^{-4}$)	Dislocation Density δ ($lin\ m^{-4}$)
Pure KDP	0.1102	17.30	1.25	2.72E-02	4.36E-02
	0.0288	23.80	4.86	7.05E-03	2.92E-03
	0.0576	30.65	2.46	1.39E-02	1.13E-02
KDP + Cy 1%	0.0394	17.35	3.52	9.74E-03	5.57E-03
	0.0298	23.84	4.70	7.29E-03	3.12E-03
	0.0672	30.69	2.11	1.62E-02	1.54E-02
KDP + Cy 2%	0.0315	17.38	4.40	7.78E-03	3.56E-03
	0.0384	23.83	3.64	9.39E-03	5.18E-03
	0.0960	30.68	1.48	2.31E-02	3.15E-02

3.2 Thermogravimetric Analysis (TGA):

Thermogravimetric analysis is a powerful tool for determining a sample's thermal stability [13]. It provides information on phase transitions, if any, the water of crystallization, and the crystal's decomposition stages. Thermal analysis was conducted on pure, and L-Cysteine doped KDP crystals in the temperature range of 20 °C to 600 °C. The pure KDP crystal

is thermally stable up to 222 ℃, as shown in figure 3(a). Pure KDP's major weight loss was about 11.67%, and since the crystals have good thermal stability up to 222 ℃, they can be used in laser processing applications where crystals must withstand high temperatures. The thermogram shows that as the temperature rises, the compound gradually decomposes. At 280 °C, a prominent endothermic peak is observed. The thermogram of L-Cysteine (1 mol%) doped KDP crystal is shown in figure 3(b). The doped crystal is more thermally stable than pure KDP, with stability reaching up to 230 ℃, which is somewhat greater than pure KDP. A significant weight loss of 11.4% was observed. At 282 ℃, the major endothermic peak is observed. The thermogram of the L-Cysteine (2 mol %) doped KDP crystal is shown in figure 3(c). It reveals that the KDP crystal doped with 2 mol% L-Cysteine is stable up to 236 ℃. In conclusion, the thermal stability temperature of the crystal increases as the doping level increases. In this instance, a significant weight decreases of 12.3% was noted, and at 289℃, the primary endothermic peak is observed.

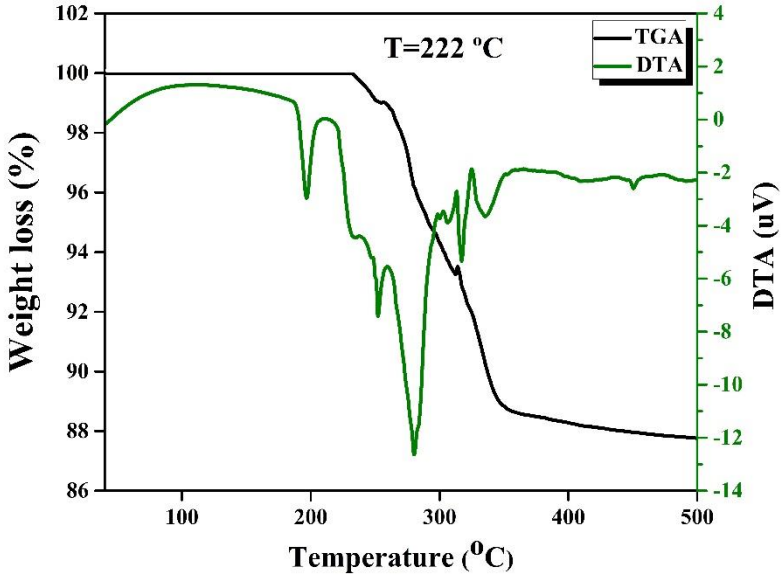

Figure 3(a). TGA-DTA curve of pure KDP crystal

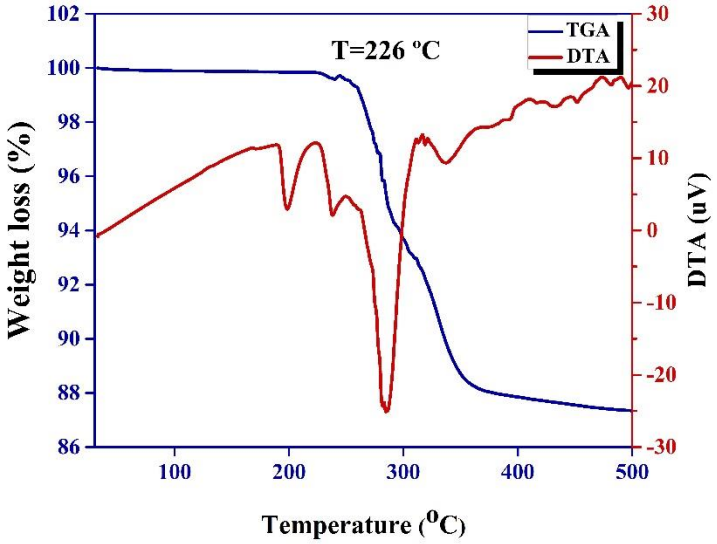

Figure 3(b). TGA-DTA curve of L-Cysteine (1 mol%) doped KDP crystal

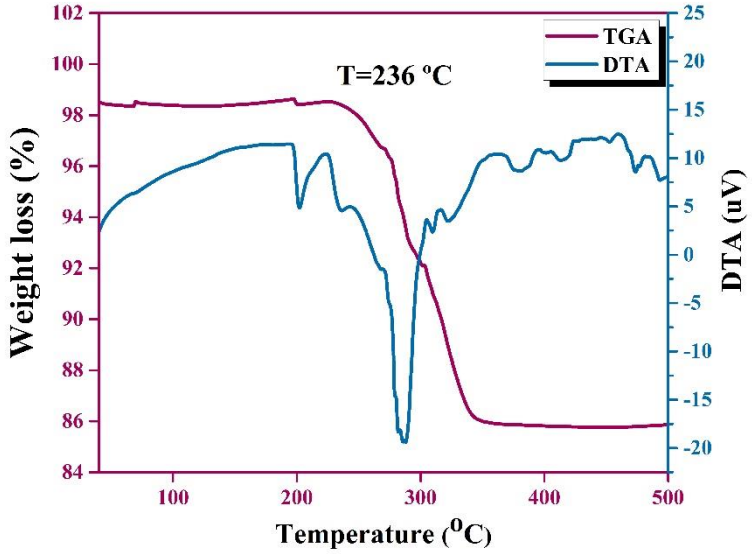

Figure 3(c). TGA-DTA curve of L-Cysteine (2 mol%) doped KDP crystal

It has been found that adding amino acids; notably, L-Cysteine, can improve the thermal stability of this important crystal. The L-Cysteine (1 mol% and 2 mol%) doped KDP crystals decompose faster than the pure KDP crystal. On the other hand, the doped samples begin to decompose slowly right at the start of the heating cycle. The sharpness of the peak indicates good crystallinity of the sample.

3.3 Dielectric Analysis:

In the frequency range of 100 Hz to 100 kHz, dielectric studies of pure KDP and L-Cysteine doped KDP crystals were performed. The applied field frequency affects the dielectric constant (ε_r) and dielectric loss. Figures 4(a-b) below illustrate this relationship. With

increasing frequency, the dielectric constant (ε_r) and dielectric loss decrease. The contribution of all four polarizations, namely electronic, ionic, orientational, and space charge, is substantial in the lowest frequency range, resulting in a high value of dielectric constant (ε') [14]. Because of the inertia of the molecules and ions, the dielectric constant (ε') tends to fall at high frequencies, making ionic and dipolar polarizations weaker or nearly absent [15,16]. Dielectric loss has the same behaviour, and its low value indicates that the crystals are of excellent quality and include less electrically active defects.

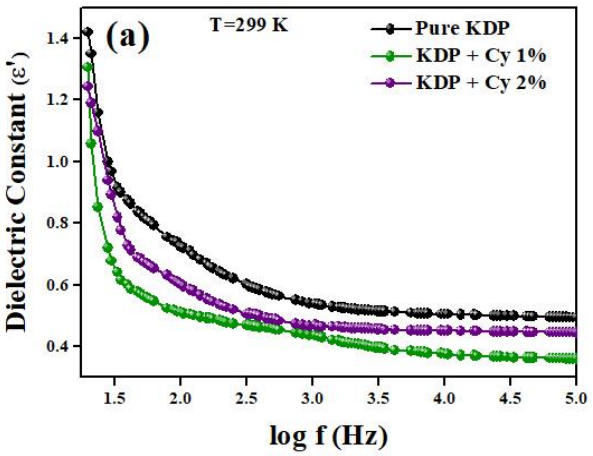

Figure 4(a). The dielectric constant of pure and L-Cysteine doped KDP crystals

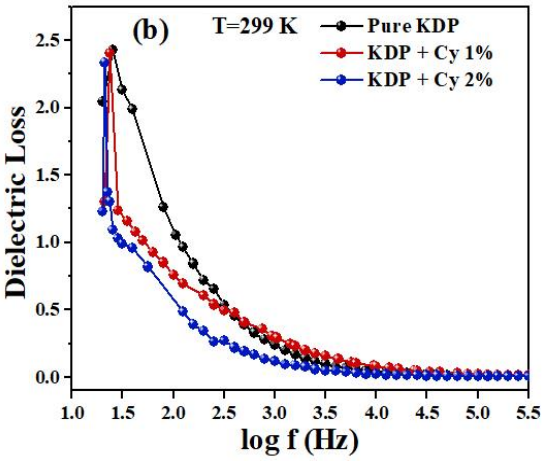

Figure 4(b). The dielectric loss of pure and L-Cysteine doped KDP crystals

As doped crystals contain fewer dipoles per unit volume than pure KDP crystals, they have a lower dielectric loss and dielectric constant, resulting in lower losses. As a result, doped crystals may be more helpful for high-speed electro-optic modulations than pure KDP crystals. Microelectronics and NLO applications depend heavily on these factors [13]. Photonic and NLO devices can benefit from materials having a low dielectric constant at high frequencies. The dielectric constant decreases with increasing percentage doping, indicating that the crystals might be ideal for electro-optic applications needing low dielectric constants.

Figures 4(c-d) demonstrate variations in resistivity and conductivity with frequency. The a. c resistivity ($\rho_{a.c}$) of the crystals decreases steadily with increasing frequency, as predicted, while the a. c conductivity ($\sigma_{a.c}$) of the crystals shows the opposite trend.

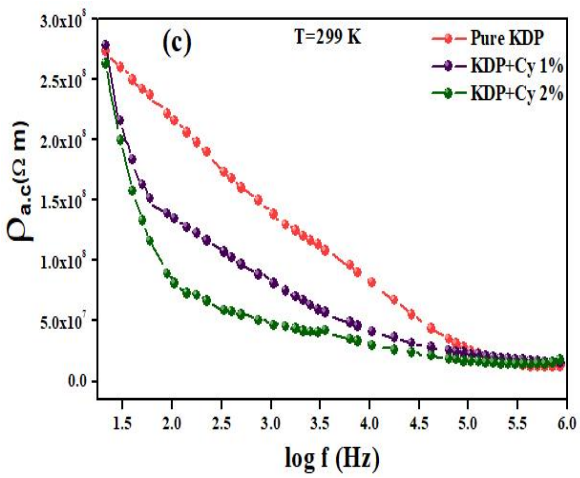

Figure 4(c). Resistivity measurements of pure and L-Cysteine doped KDP crystals

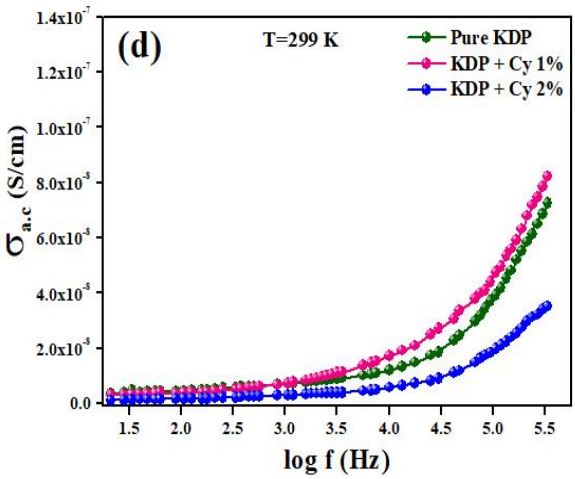

Figure 4(d). Conductivity measurements of pure and L-Cysteine doped KDP crystals

3.4 Photoluminescence (PL) Analysis:

The nature of the crystal's point or lattice defects can be determined using photoluminescence (PL) analysis. Through colour centre emissions, fluorescence analysis helps study intrinsic impurities in organic and inorganic compounds [17]. The study of photoluminescence emission at specific wavelengths is a beneficial technique for investigating crystal composition, qualitative impurity incorporation and optical phenomena such as carrier recombination [18]. Several forms of intrinsic lattice defects have been found in pure KDP crystals, which can be detected using optical spectroscopy and electron spin resonance. The simplest defects are the orientational defects of the L and D types.

Unoccupied hydrogen bonds are classified as L-type defects, while double-occupied hydrogen bonds are classified as D-type defects [19,20]. Free radicals (the so-called A and B radicals) were found in the crystals of the KDP group at temperatures below the Curie points. When one of the protons in a hydrogen bond is lost, an A radical is formed by a typical anionic group ($H_2PO_4^-$), and this defect is a hole localized at an oxygen ion near a hydrogen vacancy. A self-trapped hole B≡($[H_2PO_4]^0$) is the B radical (hole trapped by an anionic group ($H_2PO_4^-$). The trapping of an electron at the corresponding trapping centre should co-occur with the formation of a self-trapped hole [21,22]. The photoluminescence emission spectra of pure and L-Cysteine doped KDP crystals are shown in figure 5(a). The PL excitation wavelength is 247 nm, and the excitation in the crystal transparency region is induced by hydrogen vacancies (L-defect) associated with heterovalent impurities. As seen in table 3, the spectra display two emission peaks at different wavelengths.

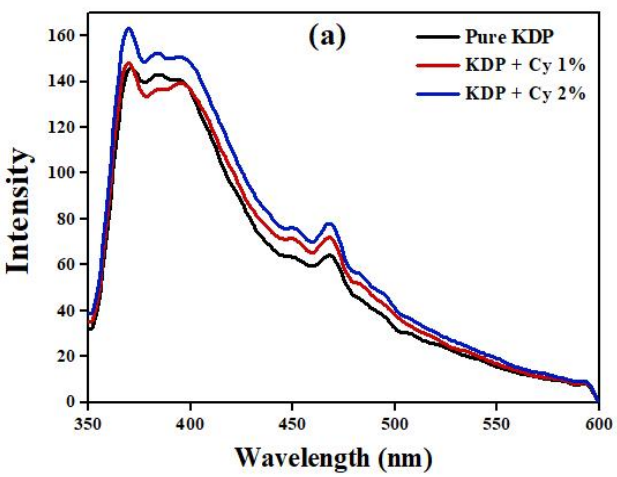

Figure 5(a). PL Emission spectra of pure and L-Cysteine doped KDP crystals

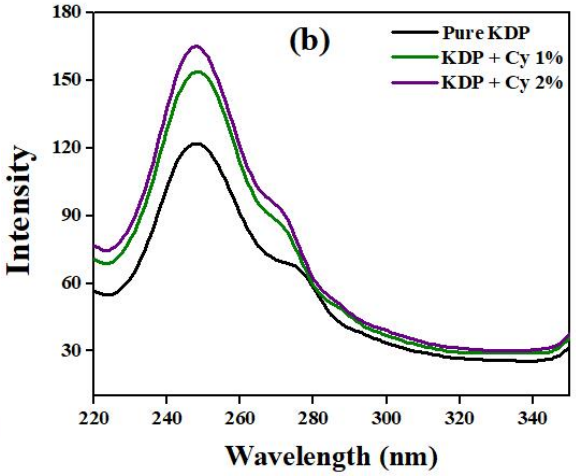

Figure 5(b). PL Absorption spectra of pure and L-Cysteine doped KDP crystals

The electrical conductivity of the material is related to the intensity of the PL emission spectrum. With the increase in concentration of L-Cysteine, the intensity of PL emission spectra is observed to decreased, implying that dopant (L-Cysteine) was incorporated into pure KDP. Electron recombination on the trapped hole centre based on hydrogen vacancy ('A' - radical or L-defect) causes the emission peak around (367-369nm), and the emission peak (467-468nm) is produced by hole recombination at the electron centre based on a double occupied hydrogen vacancy ('B'-radical or D-defect).

Table 3. PL emission peaks of pure and L-Cysteine doped KDP crystals

Sample	Emission Wavelength (nm)	
Pure KDP	368.97	468.19
KDP + Cy 1%	369.98	467.81
KDP + Cy 2%	367.90	468.00

The PL absorption spectra of pure and L-Cysteine doped KDP are seen in figure 5(b). When the positions of the band maxima of the absorption and emission spectra in a given material for same electronic transitions differ wavelengths, the Stokes shift takes place [23]. When the energy of an emitted photon is less than that of an absorbed photon, Stokes shift takes place. When the energy of an emitted photon is greater than that of an absorbed photon, an anti-Stokes shift takes place [24]. In solid materials, the vibrational energy (or population) relaxation causes the Stokes shift [25], and this relaxation of molecules usually occurs due to

interaction with the surroundings of a lattice site. The lattice creates a continuous intermolecular motion that will annihilate the energy of the vibrational relaxer, resulting in lattice motion excitation at higher levels of energy [26].

Table 4 shows that increasing the dopant concentration of 2 mol% L-Cysteine causes a slight increase in the Stokes shift compared to pure KDP. This type of behaviour can be explained in the following way: The dopant L-Cysteine forms a dipole with a positive NH^{3+} and a negative COO^{-} charge surrounding the KDP lattice. The dipole moment of L-Cysteine changes as it reaches the excited state under the influence of electromagnetic radiation; however, the KDP lattice adjusts to it quickly. As a result, when the system experiences vibration relaxation, the dipole moments will realign with the applied optical field. As a result, increasing the dopant concentration of L-Cysteine would make it easier for the KDP lattice to realign, decreasing the Stokes shift in ascending order of up to a certain doping percentage.

Table 4. Stokes shift variation of pure and L-Cysteine doped KDP crystals

Sample	Energy Absorption (eV)	Energy Emission (eV)	Stokes shift
Pure KDP	5.0030	3.3452	1.6578
KDP + Cy 1%	4.9959	3.3574	1.6385
KDP + Cy 2%	5.0066	3.3566	1.6500

3.5 Fourier Transform Infrared (FT-IR) Spectroscopy:

The Fourier transform infrared analysis was carried out in 4000 cm^{-1} and 500 cm^{-1} wavenumbers to reveal the amino acid complex co-ordination. Infrared spectroscopy is a diverse and versatile technique, and one of the most significant characteristics of infrared (IR) spectroscopy is its qualitative aspects. The results obtained testify that all the IR spectra are practically identical and agree with the available literature data [27]. The bond assignments confirm that various functional groups are present in the material and are tabulated in table 4. Figure 6 shows the infrared spectra of pure, and L-Cysteine doped KDP crystals. The FTIR spectra show the interaction between host KDP and the grafted amino acid. The additional peaks found in L-Cysteine doped KDP crystal spectra correspond to the functional groups of L-Cysteine, confirming its presence in the KDP crystal lattice. However, there is a slight shift in the peak positions because of the hydrogen bonds. The absence and inclusion of peaks and the broadening and change in the vibrational absorption frequencies in the FTIR spectra signify the presence and inclusion of the dopant into the lattice site of KDP. Since the KDP bonds

overlap the amino acid vibrations, some of the frequencies are subtly shifted. The stretching, bending, twisting, and rotating vibrational modes of atoms in a molecule was analyzed in FTIR experiments to classify the functional group of the samples. The presence of coordinated bond changes in the FTIR spectrum suggests that L-Cysteine has been integrated into the KDP crystal lattice. Some $[H_2PO_4]^-$ bands overlap with amino acid vibrations in the spectra of amino acid doped crystals. As a result, a few hydrogen phosphate ionic bonds broaden, and certain frequencies change slightly.

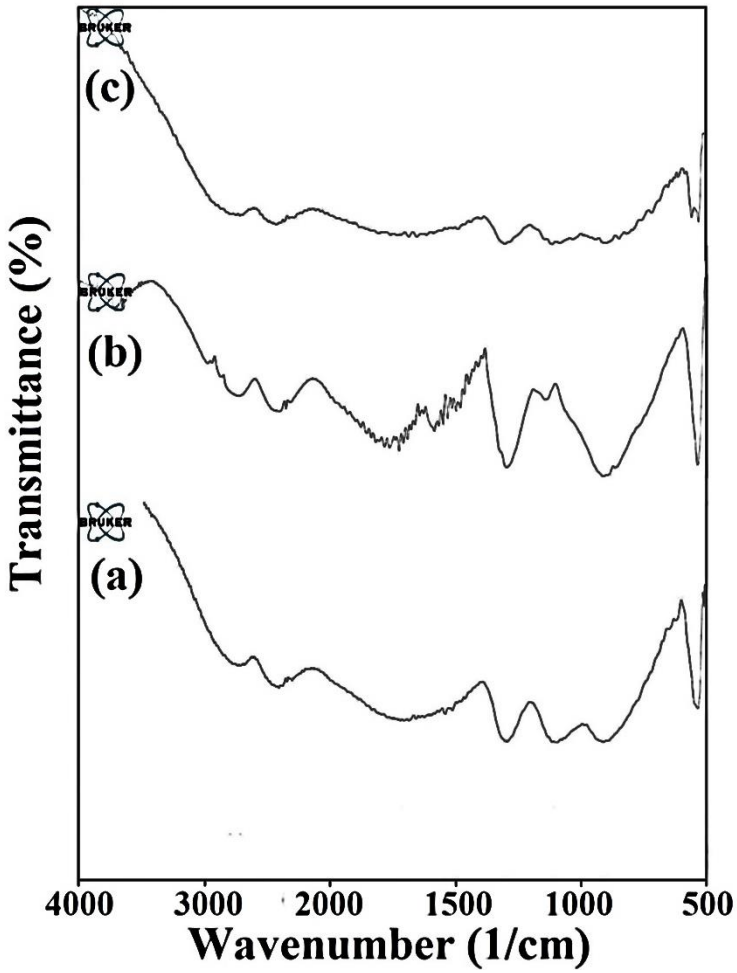

Figure 6. FTIR of **(a)** pure KDP, **(b)** L-Cysteine (1 mol%) doped KDP crystal and **(c)** L-Cysteine (2 mol%) doped KDP crystal

The force constant of different bond vibrations present in the sample can be calculated using an equation relating absorption frequency and force constant:

$$\upsilon = 1330 \sqrt{F\left(\frac{1}{M_1} + \frac{1}{M_2}\right)} \quad (1)$$

where, υ = Absorption frequency (cm^{-1}), F= Force constant ($N\ m^{-1}$), 1330 = $(N_A \times 10)^{1/2}/2\pi C$, N_A = Avogadro number and M_1 and M_2 are Molecular masses of atoms (u)[28].

Table 3. Characteristic Absorption Frequencies of Various Functional Groups

Bond Assignments	**Wavenumber (cm^{-1})**		
	Pure KDP	**KDP + Cy 1%**	**KDP + Cy 2%**
O-H vibration	3321	3323	3322
N-H stretching	-	2920	2921
O-H asymmetric stretching	2927	2923	2921
O-P-OH symmetric stretching	1704	1645	1651
O=P-OH stretching	1629	1630	1631
N-C-N stretching	-	1685	1684
NH_3 bending	-	1449	1451
C-COO^- symmetric stretching	-	1412	1412
C-N-H stretching	-	1298	1299
P=O stretching	1295	1298	1300
P-O-H symmetric stretching	909	913	913
COO^- bending	-	613-677	613-675
HO-P-OH bending/CH_2-CH-N bending	533	537	529

Table 4. The calculated value of force constant of O-H vibration for pure and doped KDP crystals.

Sample	**Absorption Wavenumber (cm^{-1})**	**Force Constant (Nm^{-1})**
Pure KDP	3321	591.14
KDP + Cy 1%	3323	591.86
KDP + Cy 2%	3322	591.50

3.6 Ultraviolet-Visible (UV-Vis) Spectroscopy:

Figure 4 depicts the optical transmittance spectra obtained. In order to fabricate optical devices, the crystal must be highly transparent over a broad wavelength spectrum [29,30]. The crystals' overall high transmittance in the visible region is suitable for the second harmonic

generation and NLO devices [31,32]. The absorption coefficient (α) is calculated from the transmittance data using the following expression,

$$\alpha = \frac{\log_{10}\left(\frac{1}{T}\right)}{t} \quad (2)$$

where, t = Thickness of the crystal and T= Transmittance

The bandgap can be calculated using the dependence of the optical absorption coefficient on photon energy [33].

$$\alpha h\upsilon = A\,(h\upsilon - E_g)^2 \quad (3)$$

where, A = Constant, h = Planck's constant, α = Absorption Coefficient, υ = Frequency and E_g= Optical Bandgap

Figure 5 shows $(\alpha E)^2$ versus E (Tauc's plot) for pure KDP and 1 mol% and 2 mol% L-Cysteine doped KDP crystals, where E = Photon Energy and α= Absorption Coefficient. The energy bandgap (E_g) was calculated by extrapolating the linear component of the spectrum to the high energy side. The bandgap of KDP increases from 3.41 eV to 4.40 eV and 4.50 eV at 1 mol% and 2 mol% doping levels. The KDP band gap has increased by a considerable amount. Amino acid doping has been shown to increase the optical bandgap, for example, in ADP (Ammonium Dihydrogen Phosphate), suggesting increased SHG performance [34]. The crystals have a high transmittance in the visible edge to IR regions due to the wideband difference, indicating their suitability for photonic and optical applications [35].

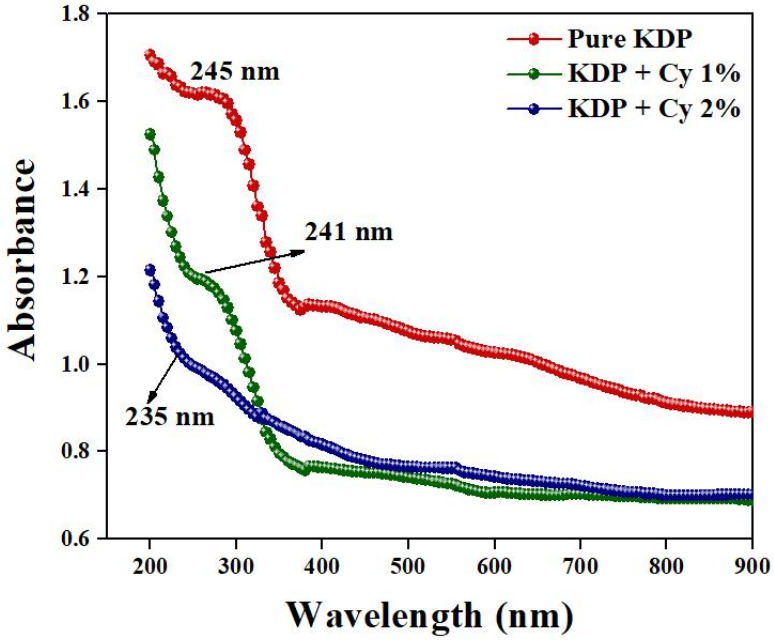

Figure 4. UV-Vis spectra of pure and L-Cysteine doped KDP crystals.

The cut-off wavelengths of the L-Cysteine 1 mol% and L-Cysteine 2 mol% doped KDP crystals were also observed to be around 241 nm and 235 nm, respectively; however, the cut-off wavelength of pure KDP was observed to be around 245 nm. UV-tunable lasers and NLO system applications can benefit significantly from doped KDP crystals with high transmittance and a changed cut-off wavelength [36]. The study of optical constants plays a vital role in determining the crystals' suitability for various optoelectronic applications [37].

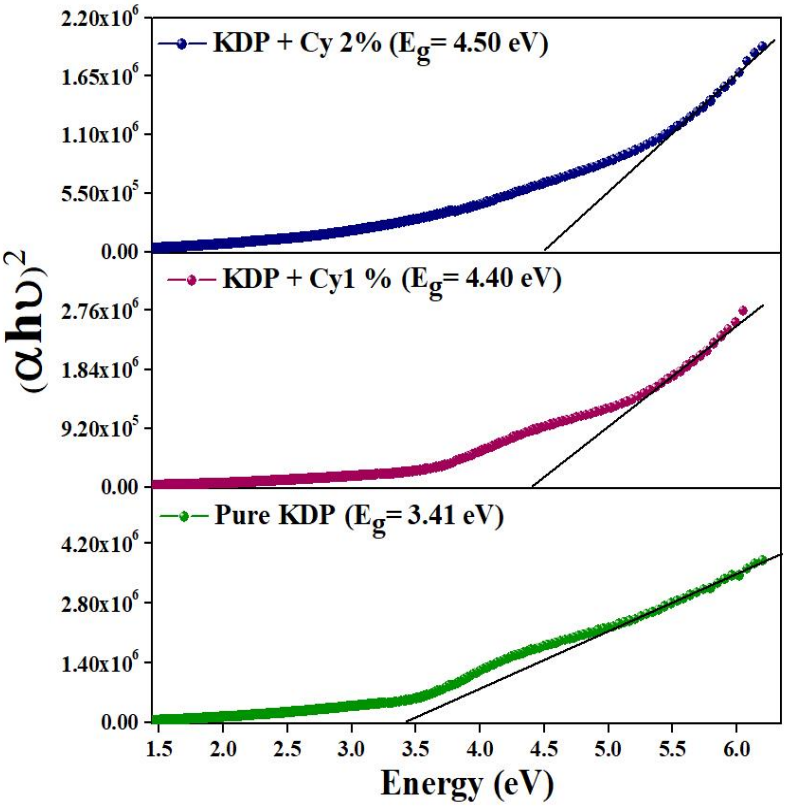

Figure 5. Tauc's plot and band gaps of pure and L-Cysteine doped KDP crystals

The refractive index is an optical constant that determines how light deviates in a medium and plays a crucial role in describing light-matter interactions. For crystals, the refractive index should be smaller. The following theoretical equations were used to derive the additional optical constants: extinction coefficient, reflectance, refractive index, complex dielectric constant and optical conductivity [38,39].

With the help of the absorption coefficient, the value of the extinction coefficient is calculated,

$$K = \frac{\lambda\alpha}{4\pi} \tag{4}$$

The reflectance was calculated in terms of absorption coefficient,

$$R = \frac{1 \pm \sqrt{(1 - exp(-\alpha t) + exp(\alpha t))}}{1 + \exp(-\alpha t)} \tag{5}$$

and the linear refractive index (η) is calculated as follows:

$$\eta = \frac{1}{T} + \sqrt{\left(\frac{1}{T} - 1\right)} \tag{6}$$

Here, the complex dielectric constant is associated with the refractive index and the extinction coefficient,

$$\varepsilon_c = \varepsilon_r + \varepsilon_i \tag{7}$$

where, the real and imaginary dielectric constant is given by $\varepsilon_r = \eta^2 - K^2$ and $\varepsilon_i = 2\eta K$.

When a material is irradiated with light, its optical conductivity is a measure of its frequency response:

$$\sigma_{o.p} = \frac{\alpha \eta c}{4\pi} \tag{8}$$

where, c is the speed of light.

Figure 6 shows the photonic response of the refractive index of the crystals grown. It can be shown that the refractive index of KDP crystal has changed due to the addition of L-Cysteine, making doped KDP crystals quite a suitable photorefractive material for holographic data storage systems [40]. Also, a crystal with a low refractive index is in high demand for coating solar thermal devices [41] and calibrating the merit of photonic device components [42].

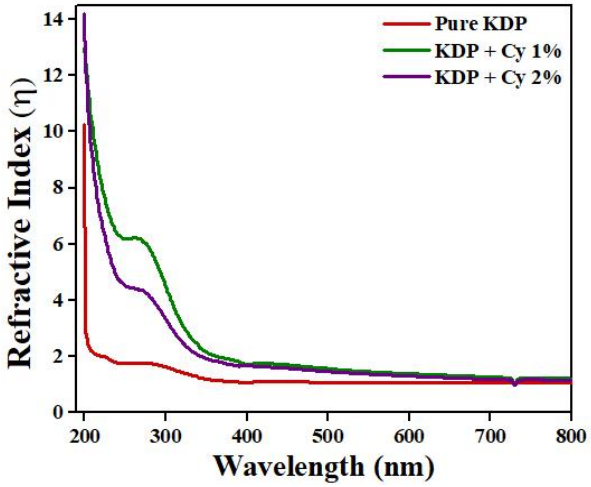

Figure 6. Refractive index of pure and L-Cysteine doped KDP crystals

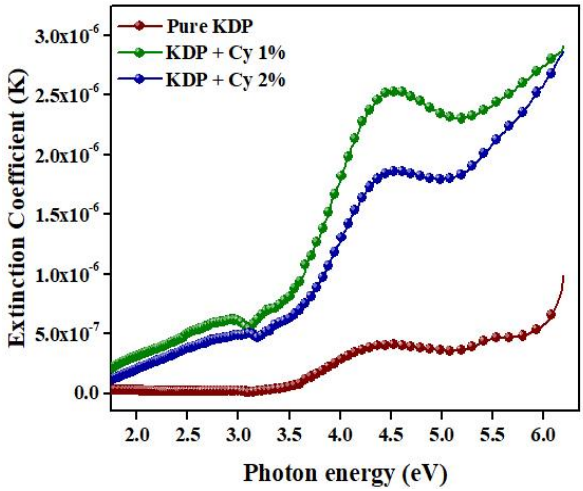

Figure 7. The extinction coefficient of pure and L-Cysteine doped KDP crystals

The optical loss in a material medium is determined by the extinction coefficient of the material, which is the most important parameter for controlling the frequency of the optical signal. The extinction coefficient and optical conductivity of L-Cysteine doped KDP crystals in the high photon field increase compared to those of pure KDP crystals, as seen in figures 7 and 8. The extinction coefficient of all the crystals rises as photon energy increases, implying that the fractional loss of radiation incident on the crystal increases with increasing photon energy. This might be due to scattering and absorption behaviours depending on photon energies and scattering centre type. Compared to pure KDP, the magnitude of the extinction coefficient is much larger and uniform for L-Cysteine doped KDP. The higher the optical conductivity, the better the material's conversion efficiency.

The amount of electromagnetic radiation that penetrates a substance is measured by the skin depth (δ). It is defined numerically as,

$$\delta = \frac{1}{\alpha} \tag{9}$$

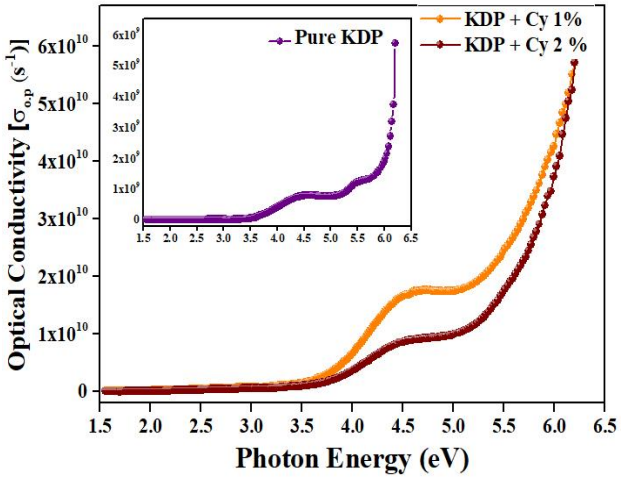

Figure 8. Optical Conductivity of pure and L-Cysteine doped KDP crystals

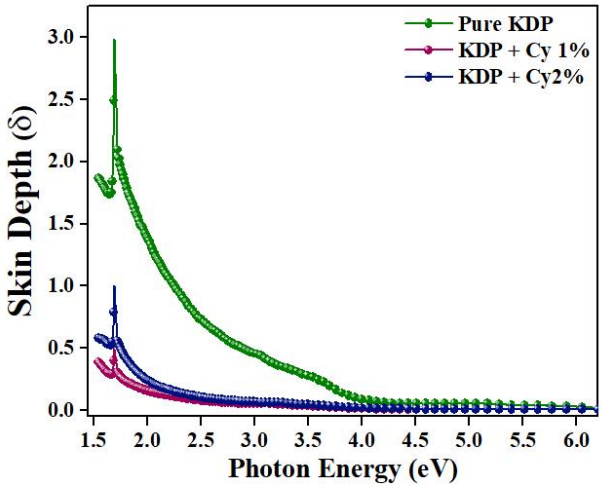

Figure 9. The skin depth variation with a photon energy of pure and L-Cysteine doped KDP crystals

The variation in skin depth with photon energy for pure and L-Cysteine doped KDP crystals is shown in figure 9. For all the crystals, the skin depth increases slightly with a prominent peak in the lower photon energy region (near 1.70 eV) and subsequently falls as the photon energy increases; however, this behaviour becomes more insignificant as the doping increases. With an increase in L-Cysteine doping concentration in KDP crystal, the magnitude of skin depth decreases, and these results suggest that the skin depth of the crystals is related to their transmittance [43]. L-Cysteine doping in KDP crystals could be more useful as implied these findings. It is also worth noting that the entire region excludes absorption bands, resulting in excellent transparency in the visible spectrum. As a result, the material's optical properties confirm its applicability for NLO, optoelectronic, and photonic applications.

3.7 Relative Second Harmonic Generation (SHG) Efficiency:

The Kurtz and Perry powder technique is advantageous for the initial testing of materials for a second harmonic generation. The SHG property of the crystals was tested using a fundamental beam of wavelength 1064nm from a Q-switched Nd: YAG laser. The pure and L-Cysteine added KDP crystals were ground into a fine powder and packed into microcapillary tubes placed in the direction of laser pulses with a pulse width of 10 ns and a repetition rate of 10 Hz, input energy being 1.2 mJ/pulse. The green emission of wavelength 532 nm from the sample indicates second harmonic generation. In this experiment, the powdered potassium dihydrogen phosphate was used as a reference. The output to input power ratio was used to calculate the SHG efficiency values shown in table 5. We may say that this increase in SHG

efficiency of KDP with the addition of L-Cysteine is because L-Cysteine has NH^{3+} and COO^{-} groups. It is evident from these results that doping of KDP with L-Cysteine improves its SHG performance and that the doped crystals are more suitable for laser-related system applications than the pure crystals.

Table 5. Comparison of relative SHG efficiency of pure and L-Cysteine doped KDP crystals

Sample	Relative SHG efficiency
Pure KDP	-
L-Cysteine (1 mol%) doped KDP	2.5
L-Cysteine (2 mol%) doped KDP	2

4. Conclusion:

At room temperature, pure KDP and L-Cysteine (1 mol% and 2 mol%) doped KDP crystals have been successfully produced with good perfection using the slow evaporation method. Moreover, the crystals were transparent. The Powder XRD investigation suggests the single-phase nature and defect induced by the dopant in KDP. It has been observed that there is a slight increase in the lattice strain of doped KDP crystals. According to the TGA study, amino acid added to pure KDP crystal improves its thermal stability; however, it decomposes faster than pure KDP crystal. The dielectric study reveals that L-Cysteine doping in KDP crystals reduces its electrical characteristics, such as dielectric loss, dielectric constant and conductivity, making it acceptable for microelectronic applications. The PL emission spectra of pure and doped KDP crystals show that L- and D- defects exist in doped and pure crystals. The electron and hole recombination at various photon energies has also been observed in PL emission spectra. The existence of Stokes shift and vibration relaxation phenomena indicates that doping has caused defects in KDP. The FT-IR spectra confirm the presence of all fundamental functional groups of KDP.

In the UV-Visible and IR regions, the doped crystals have excellent transmittance, with an average of 90%. L-Cysteine doped KDP crystals have a low cut-off wavelength and wide transparency (entire visible region), making them ideal for generating short-wavelength laser light in the UV-Vis region (due to the frequency doubling phenomenon). With doping levels of 1 mol% and 2 mol%, L-Cysteine in KDP crystals improves the bandgap from 3.41 eV to 4.40 eV and 4.50 eV, respectively, making it more appropriate for SHG application. The large magnitude of optical conductivity (10^{10} s^{-1}) indicates that the material has a very

high photo-response nature. The SHG efficiency of L-Cysteine doped KDP (1 mol%) crystal is 2 times that of pure KDP, implying that it could be used in frequency conversions and other applications. Thus, L-Cysteine doping improves the linear and nonlinear optical performance of KDP crystals, indicating that the doped crystals are promising candidates for diverse NLO applications.

References:

1. R. A. Laudise, R. Ueda and J. B. Mullin (Eds.), "*Crystal Growth and Characterization"*, North-Holland Publishing Company, Amsterdam (1975) pp. 255-277.
2. H. S. Nalwa, S. Miyata, "*Nonlinear Optics of Organic Molecules and Polymers"*, CRC Press, New York (1997).
3. S. B. Monaco, L. E. Davis, S. P. Velsko, F. T. Wang, D. Eimerl, *J. Cryst. Growth*, **85** (1987) pp. 252-255.
4. J. Podder, *J. Cryst. Growth*, **237-239** (1) (2002) pp. 70-75.
5. H. Endert and W. Melle, *Phys. Stat. Solidi*, **74** (1982) pp. 141-148.
6. H. V. Alexandru, S. Antohe, *J. Cryst. Growth*, **258** (2003) pp. 149-157.
7. H. V. Alexandru, *J. Cryst. Growth*, **166** (1996) pp. 162-166.
8. V. I. Bredikhin, G. L. Galushkina, A. A. Kulagin, S. P. Kuznetsov, O. A. Malshakova, *J. Cryst. Growth*, **259** (2003) pp. 309-320.
9. N. A. Booth, A. A. Chernov, P. G. Vekilov, **237-239**(3) (2002) pp. 1818-1824.
10. N. Gupta and V. Voloshinov, *J. of Optics, IOP*, **16** (2014).
11. M. J. Gunning, R. E. Raab, W. Kucharczyk, *J. Opt. Soc. Am. B*, **18**(8) (2001) pp. 1092-1098.
12. Mohd. Anis, M. D. Shirsat, G. G. Muley and S. S. Hussaini, *Physica B: Condensed Matter*, **449** (2014) pp. 61-66.
13. V. Kannan, K. Thirupugalmani, G. Shanmugam and S. Brahadeeswaran, *J. Therm. Analysis and Calorim.*, **115** (2013) pp. 731-742.
14. N. V. Prasad, G. Prasad, T. Bhimasankaram, S. V. Suryanarayana and G. S. Kumar, *Bull. of Mater. Sci.*, **19** (1996) pp. 639-643.
15. S. M. Dharmaprakash and P. Mohan Rao, *J. Mater. Sci. Lett.***8**, 1167-1168 (1989).
16. K. V. Rao and A. Samakula, *J. Appl. Phys.*, **36** (1965) pp. 2031-2038.
17. V. Subhashini, S. Ponnusamy, C. Muthamizhchelvan, *J. Cryst. Growth*, **363** (2013) pp. 211-219.
18. T. H. Gfroerer, "*Photoluminescence in Analysis of Surfaces and Interfaces, Encyclopedia of Analytical Chemistry"*, John Wiley & Sons Ltd. (2006) pp. 1-23.
19. N. Ogorodnikov, V. A. Pustovarov, B. V. Shul'gin, V. T. Kuanyshev and M. K. Satybaldieva, *Opt. Spectrosc*., **91** (2001) pp. 224-231.

20. N. Orogodnikov, V. Yu. Yakovlev, B. V. Shul'gin and M. K. Satybaldieva, *Phys. Solid State*, **44** (2002) pp. 880-887.

21. N. Orogodnikov, M. Kirm, V. A. Pustovarov and V. S. Cheremnykh, *Opt. Spectrosc.*, **95** (2003) pp. 385-389.

22. N. Orogodnikov, V. A. Pustovarov, M. Kirm and V. S. Cheremnykh, *Opt. Spectrosc.*, **97** (2004) pp. 244-250.

23. J. R. Gispert, *"Co-ordination Chemistry"*, Wiley -VCH (2008) pp. 483.

24. A. Kitai, *"Luminescent Material and Application"*, Wiley (2008) pp. 32.

25. F. Hiroshi, J. E. Straub, *PNAS*, **102** (2005) pp. 6726-6731.

26. A. Takmakoff, *"Lecture notes on Vibrational Relaxation"*, Introduction to Quantum Mechanics II, MIT Department of Chemistry (2009).

27. N. Cabera, D. A. Vermilyea, "*The growth of crystals from solution, Growth and Perfection of Crystals"*, New York: Wiley; London: Chapman & Hall (1958) pp. 393-410.

28. N. B. Colthup, L. H. Daland S. E. Wiberley, "*Introduction to Infrared and Raman Spectroscopy"*, Academic Press, London, (1975).

29. V. Krishnakumar and R. Nagalakshmi, *Spectrochimica Acta Part A*, **61**(3) (2005) pp. 499-507.

30. V. Krishnakumar and R. J. Xavier, *Spectrochimica Acta Part A*, **60**(3) (2004) pp. 709-714.

31. S. AnieRoshan, C. Joseph, M. A. Ittyachen, *Mater. Lett.*, **49** (2001) pp. 299-302.

32. V. Venkataramanan, S. Maheswaran, J. N. Sherwood, H. L. Bhat, *J. Cryst. Growth*, **179** (1997) pp. 605-610.

33. N. Tigau, V. Ciupinaa, G. Prodana, G. I. Rusub, C. Gheorghies and E. Vasilec, *J. of Optoelectronics and Adv. Mater.*, **6**(1) (2004) pp. 211-217.

34. R. N. Shaikh, M. D. Shirsat, P. M. Koinkar, S. S. Hussaini, *Opt. and Laser Tech.*, **69** (2015) pp. 8-12.

35. S. Suresh, A. Ramanand, D. Jayaraman and S. M. Navis Priya, *J. of Minerals & Mater. Charactr. &Engg.*, **9**(12) (2010) pp. 1071-1080.

36. S. M. Azhar, Anis Mohd., S. S. Hussaini, S. Kalainathan, M. D. Shirsat, G. Rabbani, *Optics and Laser Technology*, **87** (2017) pp. 11-6.

37. R. Robert, C. Justin Raj, S. Krishnan, R. Uthrakumar, S. Dinakaran, S. Jerome Das, *Physica B: Condensed Matter*, **405** (2010) pp. 3248-3252.

38. P. A. Henikhena, *African Phys. Rev. 2*, **68** (2008).

39. J. I. Pankove, "*Optical Processes in Semiconductors"*, Prentice Hall, New York (1971).

40. Chen Chuang-tian, Liu Guang-zhao, *Ann. Rev. Mater. Sci.*,**16** (1986) pp. 203-243.

41. N. N. Shejwal, Mohd. Anis, S. S. Hussaini and M. D. Shirsat, *Int. J. Mod. Phys. B,* **30**(23) (2016) pp. 1650159-(1-11).

42. Mohd. Anis, G. G. Muley, *Phys. Scr.*, **91** (2016) pp. 085801.

43. A. L. Allred, *J. Inorg. Nucl. Chem.*, **1** (1961) pp. 215 – 221.